Science of the Total Environment 716 (2020) 137073

Contents lists available at ScienceDirect

Science of the Total Environment

journal homepage: www.elsevier.com/locate/scitotenv

Mechanisms responsible for N_2O emissions from intertidal soils of the Yangtze Estuary

Dengzhou Gao [a,b,1], Lijun Hou [b,*,1], Min Liu [a], Xiaofei Li [c], Yanling Zheng [a,b], Guoyu Yin [a], Dianming Wu [a], Yi Yang [a,b], Ping Han [a,b], Xia Liang [a], Hongpo Dong [a]

[a] Key Laboratory of Geographic Information Science of the Ministry of Education, College of Geographical Sciences, East China Normal University, 500 Dongchuan Road, Shanghai 200241, China
[b] State Key Laboratory of Estuarine and Coastal Research, East China Normal University, 3663 North Zhongshan Road, Shanghai 200062, China
[c] Key Laboratory for Humid Subtropical Eco-geographical Processes of the Ministry of Education, Fujian Normal University, 8 Shangsan Road, Fuzhou 350007, China

HIGHLIGHTS

- Gross N_2O production and consumption degree controlled the N_2O dynamics.
- N_2O production was dominated by bacteria denitrification.
- Hydroxylamine oxidation contributed substantially to N_2O production.

GRAPHICAL ABSTRACT

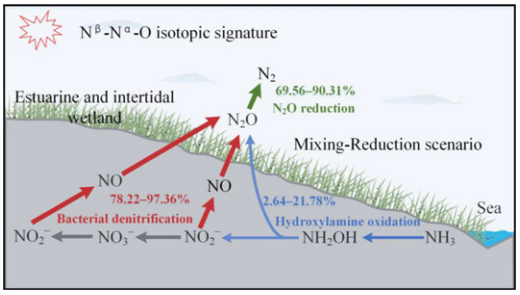

ARTICLE INFO

Article history:
Received 17 October 2019
Received in revised form 30 January 2020
Accepted 31 January 2020
Available online 1 February 2020

Editor: Jay Gan

Keywords:
Nitrous oxide
Isotope
Soils
Intertidal wetlands
Yangtze Estuary

ABSTRACT

Estuarine and coastal wetland ecosystems are important sources of atmospheric nitrous oxide (N_2O). However, the underlying driver of emitted N_2O from estuarine and coastal wetlands remains poorly understood. Here, natural-abundance isotope technique was applied to characterize the processes responsible for N_2O emission from the intertidal soils of the Yangtze Estuary. Measured N_2O emission rates ranged from 0.70 to 2.15 μmol m^{-2} h^{-1}, with relatively high values at the upper estuarine sites. The $\delta^{15}N$, $\delta^{18}O$ and SP (intramolecular ^{15}N site preference) of emitted N_2O varied from −4.5 to 6.7‰, 42.4 to 53.2‰, and 6.7 to 15.4‰, respectively. Gross N_2O production and consumption rates were within the ranges of 3.16–14.34 μmol m^{-2} h^{-1} and 2.22–-12.54 μmol m^{-2} h^{-1}, respectively, showing a similar spatial pattern to N_2O emission. N_2O consumption proportion varied from 69.56 to 90.31%, which was generally lower at the upper estuarine sites. The gross production rates and consumption degree of N_2O simultaneously controlled the variations in N_2O emission. Bacterial denitrification was the dominant production pathway (78.22–97.36%), while hydroxylamine (NH_2OH) oxidation contributed 2.64–21.78% to N_2O production. Soil pH, Fe^{2+}/Fe^{3+}, sulfide and substrate availability were probably the main factors governing the N_2O emission dynamics. Overall, these results highlight the substantial role of NH_2OH oxidation and N_2O consumption in N_2O release in redox-dynamic soils of estuarine intertidal wetlands.

1. Introduction

Nitrous oxide (N_2O) is an important greenhouse gas, which contributes nearly 10% of the total anthropogenic radiative forcing

* Corresponding author.
E-mail address: ljhou@sklec.ecnu.edu.cn (L. Hou).
[1] Dengzhou Gao and Lijun Hou contributed equally to this work.

https://doi.org/10.1016/j.scitotenv.2020.137073
0048-9697/

(Butterbach-Bahl et al., 2013). The global warming potential of N_2O is approximately 20 and 300 times greater compared with methane and carbon dioxide, respectively (IPCC, 2013). In addition, N_2O has a long atmospheric lifetime, with a half-life time of about 114 years (IPCC, 2013; Prather et al., 2015). It is also a key chemical affecting and destroying the stratospheric ozone layer (Ravishankara et al., 2009). Currently, the atmospheric concentration of N_2O is approximately 327 ppbv, with an average increasing rate of 0.77 ± 0.03 ppbv per year over the past several decades (Butterbach-Bahl et al., 2013; Gil et al., 2017). Therefore, understanding the mechanisms of N_2O emission is essential to advance effective management strategies for N_2O mitigation in natural ecosystems (Yang and Silver, 2016; Bourbonnais et al., 2017).

On a global scale, the dominant pathways of N_2O production in natural environments are tightly associated with microbial nitrogen (N) transforming processes such as nitrification (NIT) and denitrification (DNF) (Wunderlin et al., 2013). In the NIT process, N_2O is produced as a byproduct through oxidation of hydroxylamine (NH_2OH), an intermediate of ammonia (NH_3) transformation to nitrite (NO_2^-) (Kozlowski et al., 2014). Moreover, some ammonia-oxidizing bacteria and archaea can reduce nitrite (NO_2^-) to N_2O, a process designated as nitrifier DNF (Wrage et al., 2001). In DNF, N_2O is produced by denitrifiers as an obligatory intermediate during the reduction of nitrate (NO_3^-) to dinitrogen gas (N_2) (Toyoda et al., 2011). In addition, other biotic and abiotic processes, e.g., fungal DNF, dissimilatory nitrate reduction to ammonia and chemo-denitrification, may contribute to N_2O production (Butterbach-Bahl et al., 2013; Duan et al., 2017). However, N_2O emission is complicated because N_2O can be consumed simultaneously during the production (Vieten et al., 2007; Toyoda et al., 2011). N_2O reduction to N_2 in DNF process has been regarded as an important N_2O consumption pathway, which plays a crucial role in N_2O release (Vieten et al., 2007).

Estuarine and coastal wetlands are significant natural sources of N_2O to the atmosphere (Dong et al., 2011). Until now, numerous works have reported N_2O emission fluxes in estuarine and coastal wetlands (Amouroux et al., 2002; Wang et al., 2007; Moseman-Valtierra et al., 2011; Sun et al., 2013; Tong et al., 2013; Musenze et al., 2014; Yang and Silver, 2016), but the spatio-temporal patterns and underlying mechanisms remain largely uncertain. It is difficult to discern the drivers of N_2O dynamics only through measurements of N_2O emission fluxes and environment factors (Yang and Silver, 2016; Gil et al., 2017). Generally, N_2O production and consumption are affected mainly by the soil water content, texture, oxidative-reductive conditions, pH, and carbon and N substrate availability (Well et al., 2006; Liu et al., 2010; Köster et al., 2011; Zhu et al., 2013; Yang and Silver, 2016). Optimum conditions for N_2O production via DNF are assumed to exist at a higher soil water content, while its production at a lower water content is attributed in part to NIT (Bateman and Baggs, 2005; Well et al., 2006). N_2O production through NH_2OH oxidation is favored in O_2- and NH_4^+-enriched environments, whereas nitrifier DNF is enhanced in environments with low O_2 and high NO_2^- concentrations, especially those environments with alternating aerobic-anaerobic conditions (Wunderlin et al., 2013; Ma et al., 2017). However, the responses of N_2O production and consumption processes to environmental factors in different ecosystems are not consistent (Butterbach-Bahl et al., 2013; Quick et al., 2019). Estuarine and coastal areas are influenced by land-ocean interactions, such as alternations between salty and fresh water and between exposure and flooding, which may result in a great gradient change of physico-chemical factors and further affect the N_2O dynamics (Osland et al., 2013).

At present, natural-abundance isotope technique has often been applied to identify N_2O production and consumption processes (Toyoda et al., 2011; Ishii et al., 2014; Bourbonnais et al., 2017). Because N_2O is an asymmetric linear N-N-O molecule, the ^{15}N isotope can be present at the central N atom position (α site) or the terminal N atom position (β site) (Toyoda and Yoshida, 1999). The $\delta^{15}N^{\alpha}$ and $\delta^{15}N^{\beta}$ values of N_2O are determined by the N_2O formation mechanism, and several studies have demonstrated that the intramolecular site preference (SP, defined as the difference of $\delta^{15}N^{\alpha}$ and $\delta^{15}N^{\beta}$) values can identify the N_2O production and consumption processes (Fig. S1) (Sutka et al., 2003; Toyoda et al., 2005; Toyoda et al., 2011). This approach has been widely applied in cropland and grassland soils (Maeda et al., 2010; Wolf et al., 2015; Zhang et al., 2016), water bodies (Westley et al., 2006; Breider et al., 2015; Wenk et al., 2016) and wastewater (Wunderlin et al., 2013). Nevertheless, N_2O isotopic signature and production and consumption processes in estuarine and intertidal wetlands remain largely unknown so far.

The Yangtze Estuary is located in one of the major urbanized and industrialized regions in China. A large amount of anthropogenic reactive N has been transported to the Yangtze Estuary through the river, groundwater runoff and atmospheric deposition (Yin et al., 2017), which can affect soil microbial N cycling and N_2O dynamics. However, the association of N_2O emission with its production and consumption in the estuarine environment remains unclear. Based on the characteristics of the estuarine and intertidal wetlands, we hypothesize that N_2O emission would be higher in upper estuarine zones, and that NH_2OH oxidation may play a substantial role in N_2O production. It is also assumed that N_2O emission dynamics may be regulated by soil salinity, carbon and N substrates availabilities. Thus, the objectives of this study are (1) to investigate the soil N_2O emission rates and isotopic signatures ($\delta^{15}N$, $\delta^{18}O$ and SP) in the Yangtze estuarine and intertidal wetlands, (2) to reveal the gross N_2O production and consumption as well as their regulation on N_2O emission, and (3) to identify N_2O production pathways and explore the key factors affecting the N_2O dynamics. This study improves our understanding of the mechanisms of N_2O emission in the estuarine and intertidal wetlands.

2. Materials and methods

2.1. Study area and sample collection

The Yangtze Estuary is situated in the east coast of China (30°50′00 – 31°50′N, 120°30′ – 122°00′E; Fig. 1). This area is characterized as having a typical semitropical monsoon climate. The average annual temperature is approximately 16.0 °C, with low temperatures from December to February (winter) and high temperatures from June to August (summer). The rainfall is abundant, with an average annual precipitation of 1144 mm (Wang et al., 2007). A large amount of suspended matter is carried by the Yangtze River to the coast, of which a substantial proportion is deposited in the estuarine area and forms a wide intertidal flat (Yin et al., 2017). The tide in the Yangtze Estuary is irregularly semidiurnal with average tidal amplitudes of 2.4–4.6 m (Wang et al., 2007). The intertidal soil is generally dominated by mud and fine sand, with a mean grain size of 23.1–102.5 μm (Zheng et al., 2015). Over the past several decades, the excessive input of reactive N has resulted in severe eco-environmental issues in the Yangtze Estuary and its adjacent area, such as eutrophication and algal blooms (Yin et al., 2017).

In this study, six sites were selected for sample collection along the intertidal zone of the Yangtze Estuary, based on the salinity gradient (Fig. 1), including Luchaogang (A), Donghai (B), Bailonggang (C), Shidongkou (D), Liuhekou (E) and Xupu (F). Field surveys were conducted in January (winter) and July (summer) 2017. At each site, nine undisturbed soil cores (0–5 cm) were collected using box corers (8 cm in diameter and 10 cm in height, Fig. S2) during the ebb periods. After collection, the cores were sealed immediately with gas-tight lids, placed in a cooler at 4 °C and transported to the laboratory within 3 h. In the laboratory, the nine soil cores from each site were separated into two fractions: six of the cores were immediately incubated for determination of the N_2O emission and its isotopic signatures as well as the contribution of fungi to N_2O emission (Supporting Information), and the remaining soil cores were stored in the dark at 4 °C for later determination of soil properties and potential NIT and DNF rates.

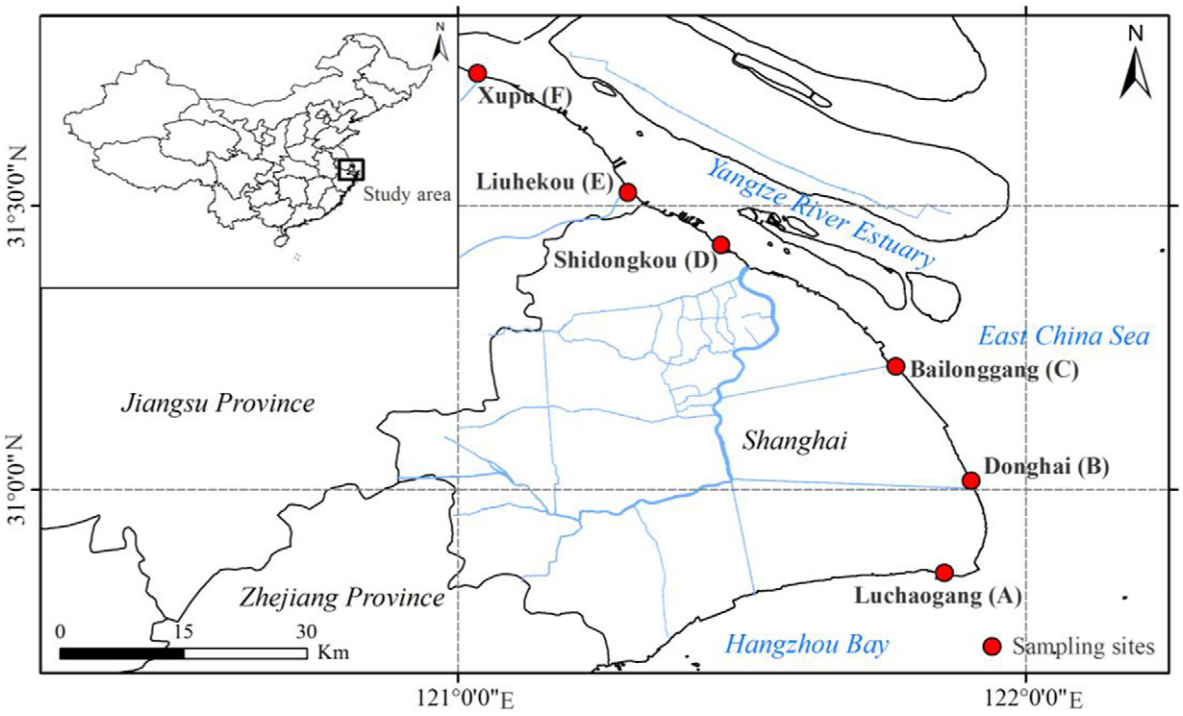

Fig. 1. Location of the study area and sampling sites.

2.2. Measurement of the soil properties, and the potential NIT and DNF rates

The soil water content and bulk density were measured by the oven-drying method and cutting-ring method, respectively (Zhang et al., 2015). The soil pH and salinity were determined using a Mettler-Toledo pH meter and a YSI-30 portable salinity meter, respectively (Yin et al., 2017). The total organic carbon (TOC) and N (TN) of the soil were measured using a Vario EL CN elemental analyzer (Elementar, Germany) after acidification with 1 M HCl (Gao et al., 2017). The soil exchangeable inorganic N, including NH_4^+, NO_3^-, and NO_2^-, was extracted with 2 M KCl, and the concentrations were determined by an automatic flow injection analyzer (Skalar Analytical SAN++, the Netherlands) (Yin et al., 2017). In addition, $\delta^{15}N$ of NH_4^+ and $\delta^{15}N$ and $\delta^{18}O$ of NO_3^- (after NO_2^- removal by sulfamic acid) were recovered by microdiffusion (Zhang et al., 2015) and denitrifier methods (Granger and Sigman, 2009), respectively, and their isotope ratios were measured on a MAT 253 Plus isotope-ratio mass spectroscopy (IRMS) facility (ThermoFinnigan, Bremen, Germany) (McIlvin and Casciotti, 2011). Therein, the international reference standards used for this study were USGS25 and IAEA N1 for NH_4^+, and USGS32, USGS34 and IAEA N3 for NO_3^-. The easily degradable organic carbon (EOC) of the soil was quantified by the method described by Song et al. (2012). The total extractable Fe and ferrous oxides (Fe^{2+}) were measured by the ferrozine method, and ferric iron (Fe^{3+}) was calculated by the difference between the total Fe and Fe^{2+} (Yin et al., 2017). The soil sulfide was determined by the methylene blue spectrophotometric method (Cline, 1969). The soil particle size was measured by laser diffraction (Mastersizer 2000, Malvern Instruments Ltd., UK).

The soil potential NIT rates were determined following the modified chlorate inhibition method (Kurola et al., 2005). Briefly, fresh soil (about 20 g) was prepared in a centrifugal tube containing 100 mL of phosphate buffer solution (pH 7.4; g/L: NaCl, 8.0; KCl, 0.2; Na_2HPO_4, 0.2; NaH_2PO_4, 0.2) with 0.5 mM $(NH_4)_2SO_4$ and 10 mM $KClO_3$, and then stirred homogeneously by a magnetic stirrer for 25 min. Triplicate slurries of each site were incubated at near-in situ temperature (32 °C for the summer and 5 °C for the winter). All tubes were shaken (150 rpm/min) continuously in the dark for 12 h, during which 5 mL of samples were drawn at 3 h intervals for NO_2^- analysis. The potential NIT rates were thus determined from the linear regression of NO_2^- accumulation over time (Kurola et al., 2005).

The soil potential DNF rates were measured by slurry experiments in combination with the isotope-tracing method (Hou et al., 2013; Deng et al., 2015). Briefly, slurries were made by mixing fresh soil and helium-purged tidal water in a volume ratio of 1:7 (soil/water). The slurry was stirred homogeneously by a magnetic stirrer for 25 min and transferred into 12-mL vials (Exetainer, Labco) and sealed with a butyl rubber stopper. Subsequently, the vials were preincubated at near-in situ temperature (32 °C for the summer and 5 °C for the winter) for approximately 36 h to eliminate the background NO_3^-, NO_2^-, and O_2. After preincubation, the vials were spiked with 100 μL sterile anoxic solutions of 12.5 mM $^{15}NO_3^-$ (^{15}N at 99%) through the septa. The final concentration of $^{15}NO_3^-$ in each vial was approximately 100 μM. Slurry incubation was stopped by adding 200 μL of a 50% $ZnCl_2$ solution to the respective vials at 3 h intervals during the total 12 h of incubation. The concentrations of $^{29}N_2$ and $^{30}N_2$ in the vials were measured by membrane inlet mass spectrometry (MIMS), and the potential DNF rates were calculated by the $^{29}N_2$ and $^{30}N_2$ production during the incubation period (Thamdrup and Dalsgaard, 2002; Deng et al., 2015).

2.3. Determination of the N_2O emission and its isotopic signatures

The intact soil cores (three replicates for each site) were sealed with gas-tight lids (equipped with three-way stopcocks) (Fig. S2), and these cores were purged with high-purity air (O_2:N_2 = 21:79 (V:V)) through the three-way stopcocks for 15 min to eliminate the background N_2O. The cores were then incubated in the dark at in situ temperatures (32 °C for the summer and 5 °C for the winter) for 6 h. Gas samples were collected using polypropylene syringes and stored in gas-tight bags at the end of each soil core incubation period. The N_2O concentration in gas samples was determined by gas chromatography (GC-2014, Shimadzu, Kyoto, Japan), and its isotopic signatures ($\delta^{15}N$, $\delta^{15}N^{\alpha}$ and $\delta^{18}O$) were determined using isotope ratio mass spectrometer (IRMS,

Isoprime100, Isoprime, Cheadle, UK) (Zhang et al., 2016). Calibration was performed using a standard reference gas produced by Air Liquide America, Specialty Gases LLC. The typical analytical precisions of $\delta^{15}N^{bulk}$, $\delta^{15}N^{\alpha}$ and $\delta^{18}O$ were 0.5‰, 0.9‰, and 0.6‰, respectively. The soil N_2O emission rates were calculated as follows (Zhang et al., 2016):

$$N_2O_{emission} = \frac{dc}{dt} \times \frac{V_H}{A_S} \times \frac{M_W}{M_V} \times \frac{T_{st}}{T_{st}+T} \quad (1)$$

where $N_2O_{emission}$ is the N_2O emission rate (μmol m^{-2} h^{-1}); $\frac{dc}{dt}$ denotes the rate of increase in the N_2O concentration inside the soil core during the incubation period (μL L^{-1} h^{-1}); V_H is the volume of the headspace (L); A_S refers to the surface area of the soil core (m^2); M_W and M_V denote the molecular weight (g mol^{-1}) and volume (L mol^{-1}) of N_2O, respectively; T is the incubation temperature (°C), and T_{st} is the standard temperature (K).

The $^{15}N^{bulk}$ and ^{18}O isotopic compositions of N_2O were expressed in δ notation with respect to the atmospheric N_2 (air) and Vienna standard mean ocean water (V-SMOW), respectively (Zhang et al., 2016). The isotope ratios were calculated as follows:

$$\delta^{15}N^{i} = \frac{^{15}R^{i}_{sample}}{^{15}R^{i}_{standard}} - 1 \ (i = bulk, \alpha, \beta) \quad (2)$$

$$\delta^{18}O = \frac{^{18}R_{sample}}{^{18}R_{standard}} - 1 \quad (3)$$

$$\delta^{15}R^{bulk} = \left(\delta^{15}N^{\alpha} + \delta^{15}N^{\beta}\right)/2 \quad (4)$$

where $^{15}R^{bulk}$ ($^{15}R^{\alpha}$ and $^{15}R^{\beta}$) and ^{18}R denote $^{14}N/^{15}N$ ($^{14}N^{15}N^{16}O/^{14}N^{14}N^{16}O$ and $^{15}N^{14}N^{16}O/^{14}N^{14}N^{16}O$) and $^{18}O/^{16}O$, respectively, and the "sample" and "standard" subscripts denote the isotope ratios of the sample and the standard atmospheric N_2 for N or Vienna Standard Mean Ocean Water (V-SMOW) for O, respectively (Zou et al., 2014). In addition, the ^{15}N SP of N_2O was calculated by the isotopic ratios as shown below:

$$SP = \delta^{15}N^{\alpha} - \delta^{15}N^{\beta} \quad (5)$$

2.4. Identification of N_2O production and consumption based on the isotopic signatures

The SP values of N_2O produced by NH_2OH oxidation and bacterial DNF are approximately 35‰ and −5‰, respectively (Toyoda et al., 2005; Sutka et al., 2006; Deppe et al., 2017). In addition, the cycloheximide addition experiments (inhibiting fungi activity, Supporting Information) showed that the N_2O production by fungi was low (Table S1), so the contribution of fungal DNF to N_2O production was not considered in this study (Maeda et al., 2017). Therefore, the contributions of NH_2OH oxidation and bacterial DNF to N_2O production were calculated from average SP values based on two-end-member mixing models as follows (Deppe et al., 2017):

$$F_{NH_2OH\ oxidation}(\%) = \frac{SP_{sample} - SP_{bacterial\ DNF}}{SP_{NH_2OH\ oxidation} - SP_{bacterial\ DNF}} \times 100\% \quad (6)$$

$$F_{bacterial\ DNF}(\%) = 100 - F_{NH_2OH\ oxidation} \quad (7)$$

where $F_{NH_2OH\ oxidation}$ and $F_{bacterial\ DNF}$ denote the soil N_2O contributions derived from NH_2OH oxidation and bacterial DNF processes, respectively; SP_{sample} is the measured SP-N_2O value; and $SP_{NH_2OH\ oxidation}$ and $SP_{bacterial\ DNF}$ represent the respective average *SP* values of NH_2OH oxidation (35‰) and bacterial DNF (−5‰) processes reported by previous studies (Toyoda et al., 2005; Sutka et al., 2006). However, Eqs. (6) and (7) are not always applicable to soil environments, especially under redox-dynamic conditions, because isotopic signatures are enriched by N_2O reduction. Here, N_2O reduction was estimated based on the SP and $\delta^{15}N$ values of N_2O (Toyoda et al., 2011) (Fig. 2). To simplify the model, we assumed that N_2O dynamics followed the Mixing-Reduction scenario (Verhoeven et al., 2019). In brief, $\delta^{15}N$ of the emitted N_2O is a function of $\delta^{15}N$ of the substrate and the isotope enrichment factor ($\varepsilon(^{15}N)_{pro}$) of the production process ($\delta^{15}N\text{-}N_2O = \delta\text{-}^{15}N_{substrate} + \varepsilon(^{15}N)_{pro}$, Toyoda et al., 2011). Therefore, the range of $\delta^{15}N\text{-}N_2O$ produced by NH_2OH oxidation and bacterial DNF in this study was estimated according to $\delta^{15}N$ of the substrate and the corresponding enrichment factor (ε), while the SP range was based on reported literature values (Yoshida, 1988; Sutka et al., 2003, 2004, 2006, 2008). Moreover, the mixing line shown in Fig. 2 was calculated from the average values of SP-N_2O and $\delta^{15}N\text{-}N_2O$ from NH_2OH oxidation and bacterial DNF, respectively (Sutka et al., 2006; Ishii et al., 2014). SP-N_2O is known to increase along with $\delta^{15}N\text{-}N_2O$ at a slope of 1.15 ± 0.12 when N_2O reduction occurs (Ostrom et al., 2007; Toyoda et al., 2011). The slope is the ratio of the fractionation factors for SP and $\delta^{15}N$ during N_2O reduction. Therefore, N_2O reduction to N_2 was taken into account using the average reduction slope and the SP and $\delta^{15}N$ values of N_2O as the origin of the reduction line. The intersection between the sample-specific reduction and mixing lines gave the estimated initial isotope values (SP^* and $\delta^{15}N^*$) of N_2O before reduction (Fig. 2). Then, the SP^* and $\delta^{15}N^*$ values of N_2O were compared with each end-member of the SP-$\delta^{15}N$ space, and the relative contributions of N_2O derived from NH_2OH oxidation and bacterial DNF were calculated by modified Eqs. (6) and (7), respectively. In addition, the approximate proportion of N_2O reduction was estimated as follows (Toyoda et al., 2011):

$$N_2O_{consumption\ proportion}(\%) = \left(1 - e^{\frac{-SP_{sample} + SP^*_{sample}}{\varepsilon(SP)red}}\right) \times 100\% \quad (8)$$

where $N_2O_{consumption\ proportion}$ denotes the proportion of N_2O reduction

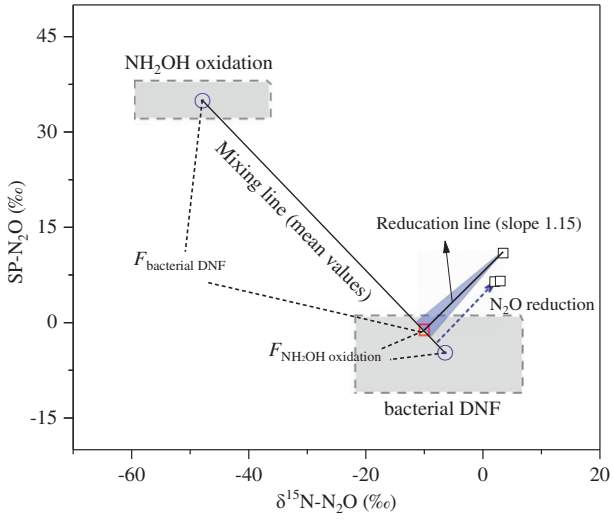

Fig. 2. An example (site A in the winter) of calculation to estimate N_2O production and consumption. The grey boxes indicate the expected ranges (SP and $\delta^{15}N$) for NH_2OH oxidation and bacterial DNF. The mixing line is drawn with mean values (blue circle) for SP and $\delta^{15}N$ values of the respective processes, and the reduction line (blue triangle indicates the range of slop for N_2O reduction) is then placed through the respective sample value (e.g. black square) to calculate the intersection (e.g. red square) with the mixing line that represent SP and $\delta^{15}N$ values of N_2O before reduction. $F_{NH_2OH\ oxidation}$ and $F_{bacterial\ DNF}$ are the contributions of NH_2OH oxidation and bacterial DNF to N_2O production, respectively.

to N_2; SP_{sample} denotes the measured SP-N_2O value, while SP^*_{sample} denotes the initial SP-N_2O value before reduction; and ε(SP)red denotes the SP enrichment factor of N_2O reduction (average of −5.9‰) (Toyoda et al., 2011). Furthermore, the gross N_2O production and consumption rates were calculated by the N_2O emission rate and consumption proportion, respectively, as follows (Toyoda et al., 2011):

$$N_2O_{\text{gross production}} = \frac{N_2O_{\text{emission}}}{100\% - N_2O_{\text{consumption proportion}}} \quad (9)$$

$$N_2O_{\text{consumption}} = N_2O_{\text{gross production}} - N_2O_{\text{emission}} \quad (10)$$

where $N_2O_{\text{gross production}}$ and $N_2O_{\text{consumption}}$ represent the gross N_2O production and consumption rates (μmol m^{-2} h^{-1}), respectively; N_2O_{emission} is the N_2O emission rate (μmol m^{-2} h^{-1}), and $N_2O_{\text{consumption proportion}}$(%) is the N_2O consumption proportion.

2.5. Statistical analysis

The data were checked for normality and homogeneity of variances, and the data were cube root- or log-converted to satisfy the assumptions for statistical testing. Repeated-measures ANOVA based on SPSS 19.0 software package (SPSS, Inc., Chicago, IL, USA) was to test the effects of sites and seasons and their interactions on all measured soil variables. Linear mixed models were performed to explore the effects of measured soil environmental parameters on N_2O emission dynamics. Soil environmental parameters were treated as fixed effects while site and season were taken as random effects (Gong et al., 2019). The collinearity between explanatory parameters was tested by the variance inflation factor (VIF). If VIF > 3 for an explanatory parameter, we removed that variable from the model (Zuur et al., 2010). Linear mixed models were conducted using the "lme" function in the "nlme" package of the R software version 3.2.2 (R Core Team, 2015).

3. Results

3.1. Soil properties and potential NIT and DNF rates

Significant spatial variabilities among the sampling sites were observed for all measured soil properties (except for $\delta^{18}O\text{-}NO_3^-$), but significant seasonal differences were only found for the water content, grain size, salinity, TN, NH_4^+, NO_3^-, and NO_2^- ($p < 0.05$, Tables 1 and S2). Soil water content and bulk density ranged from 36.27 ± 5.85 to 67.31 ± 4.08% and from 1.35 ± 0.02 to 1.50 ± 0.03 g cm^{-3}, respectively. The soils were generally characterized by a high content of fine fractions with a mean particle size of <63 μm (Table 1). Soil pH and salinity ranged from 7.31 ± 0.22 to 8.65 ± 0.08 and from 0.11 ± 0.01 to 6.61 ± 0.28, respectively, and both showed a decreasing trend from sites A to F (Table 1). The ratio of Fe^{2+}/Fe^{3+} varied from 2.14 ± 0.62 to 4.21 ± 1.19, and the maximal ratio appeared at site D (Table 1). The soil TOC and EOC concentrations varied from 8.97 ± 0.23 to 25.44 ± 3.06 g kg^{-1} and from 0.57 ± 0.05 to 2.15 ± 0.31 g kg^{-1}, respectively, and generally increased from sites A to F. A spatial distribution pattern similar to those of TOC and EOC was also observed for the soil TN (1.23 ± 0.07 to 2.39 ± 0.18 g kg^{-1}), NH_4^+ (31.45 ± 10.48 to 188.96 ± 9.88 mg kg^{-1}), NO_3^- (11.95 ± 1.38 to 19.63 ±

Table 1
Soil physicochemical characteristics (means ± standard deviation; $n = 3$).

	A		B		C		D		E		F	
	Winter	Summer	Winter	Summer	Winter	Summer	Winter	Summer	Winter	Summer	Winter	Summer
Water content (%)	62.06 ± 1.64	49.99 ± 0.41	67.31 ± 4.08	62.66 ± 2.25	51.01 ± 1.79	36.27 ± 5.85	54.71 ± 1.27	66.38 ± 4.40	62.86 ± 2.43	52.32 ± 2.50	61.41 ± 2.07	57.11 ± 2.11
Bulk density (g cm^{-3})	1.41 ± 0.04	1.44 ± 0.06	1.35 ± 0.02	1.39 ± 0.02	1.44 ± 0.02	1.50 ± 0.03	1.43 ± 0.02	1.36 ± 0.02	1.42 ± 0.05	1.38 ± 0.02	1.45 ± 0.07	1.38 ± 0.03
Mean particle size (μm)	19.45 ± 1.45	16.51 ± 1.14	17.61 ± 0.73	10.97 ± 2.77	18.97 ± 1.54	26.16 ± 2.63	16.51 ± 2.89	13.98 ± 2.32	26.15 ± 2.68	15.60 ± 1.13	16.23 ± 1.18	16.57 ± 0.86
pH	8.46 ± 0.10	8.65 ± 0.08	8.27 ± 0.07	8.35 ± 0.12	8.30 ± 0.03	8.33 ± 0.06	8.13 ± 0.08	7.72 ± 0.16	7.31 ± 0.22	7.45 ± 0.07	7.92 ± 0.09	7.65 ± 0.11
Salinity (‰)	6.61 ± 0.28	4.85 ± 0.54	5.11 ± 0.18	4.62 ± 0.23	0.40 ± 0.06	0.23 ± 0.04	0.21 ± 0.01	0.27 ± 0.06	0.14 ± 0.04	0.15 ± 0.05	0.12 ± 0.02	0.11 ± 0.01
Fe^{2+}/Fe^{3+}	2.83 ± 0.30	2.93 ± 0.46	2.63 ± 0.21	2.64 ± 0.50	2.28 ± 0.16	2.14 ± 0.62	4.21 ± 1.19	4.02 ± 0.14	2.24 ± 0.14	2.42 ± 0.33	2.21 ± 0.11	2.47 ± 0.27
TOC (g kg^{-1})	8.97 ± 0.23	9.33 ± 0.94	13.20 ± 0.86	14.89 ± 1.60	10.67 ± 1.44	9.48 ± 0.61	25.44 ± 3.06	24.72 ± 3.01	20.72 ± 1.57	14.53 ± 0.81	16.64 ± 1.77	16.45 ± 1.16
EOC (g kg^{-1})	0.89 ± 0.05	0.88 ± 0.04	1.21 ± 0.19	1.18 ± 0.10	1.60 ± 0.08	1.75 ± 0.17	0.62 ± 0.12	0.57 ± 0.05	1.88 ± 0.09	2.15 ± 0.31	1.35 ± 0.09	1.12 ± 0.11
TN (g kg^{-1})	1.23 ± 0.07	1.26 ± 0.04	1.32 ± 0.03	1.38 ± 0.02	1.19 ± 0.09	1.29 ± 0.03	2.39 ± 0.18	2.10 ± 0.40	2.20 ± 0.11	1.75 ± 0.43	1.98 ± 0.11	1.31 ± 0.04
NH_4^+ (mg kg^{-1})	36.22 ± 6.41	44.37 ± 7.90	70.54 ± 2.14	63.53 ± 6.41	43.10 ± 5.57	31.45 ± 10.48	106.32 ± 1.33	188.96 ± 9.88	89.54 ± 7.21	93.90 ± 6.07	82.66 ± 0.27	95.07 ± 8.93
NO_3^- (mg kg^{-1})	11.95 ± 1.38	12.94 ± 0.95	12.24 ± 0.58	13.09 ± 0.75	12.90 ± 0.32	13.28 ± 0.70	16.46 ± 0.12	19.63 ± 2.30	13.49 ± 0.73	14.83 ± 1.43	12.91 ± 0.39	14.61 ± 0.80
NO_2^- (μg kg^{-1})	79.81 ± 6.38	58.71 ± 9.09	93.77 ± 6.52	76.21 ± 9.10	93.19 ± 4.92	71.55 ± 6.93	183.73 ± 9.09	209.13 ± 32.04	149.61 ± 5.65	125.55 ± 10.38	137.35 ± 8.31	132.21 ± 6.80
Sulfide (mg kg^{-1})	4.35 ± 0.76	5.85 ± 0.39	3.34 ± 0.35	5.35 ± 0.61	7.25 ± 0.88	12.43 ± 2.51	94.40 ± 3.06	105.73 ± 25.30	2.39 ± 0.80	3.03 ± 0.80	1.55 ± 0.70	5.43 ± 0.98
$\delta^{15}N\text{-}NH_4^+$ (‰)	9.52 ± 0.17	8.76 ± 0.22	7.24 ± 0.91	7.49 ± 0.46	7.91 ± 0.74	7.20 ± 0.36	4.94 ± 0.49	5.17 ± 1.09	4.77 ± 1.58	5.98 ± 0.87	6.27 ± 1.04	5.68 ± 0.07
$\delta^{15}N\text{-}NO_3^-$ (‰)	16.22 ± 0.14	16.29 ± 0.35	16.33 ± 0.05	16.19 ± 0.12	16.59 ± 0.75	16.10 ± 0.21	17.01 ± 0.37	17.44 ± 0.47	18.57 ± 0.69	17.75 ± 0.60	18.08 ± 0.13	18.07 ± 0.09
$\delta^{18}O\text{-}NO_3^-$ (‰)	−1.93 ± 0.59	−2.46 ± 0.80	−1.51 ± 0.63	−2.40 ± 0.41	−2.12 ± 0.22	−2.66 ± 0.78	−2.42 ± 1.01	−3.60 ± 0.99	−3.09 ± 1.72	−1.32 ± 0.82	−2.04 ± 0.27	−2.13 ± 0.17
$\delta^{15}N\text{-}N_2O$ (‰)	6.65 ± 0.33	2.62 ± 0.38	−0.69 ± 0.51	−3.03 ± 0.62	0.70 ± 0.24	1.43 ± 0.26	−2.41 ± 0.99	−2.43 ± 0.26	−0.19 ± 0.16	−4.49 ± 0.75	−0.57 ± 0.54	−2.95 ± 0.35
$\delta^{18}O\text{-}N_2O$ (‰)	43.67 ± 0.72	43.28 ± 0.74	44.63 ± 0.67	48.54 ± 1.75	42.52 ± 0.34	47.46 ± 0.37	43.71 ± 0.27	49.29 ± 0.59	42.58 ± 0.73	51.59 ± 1.43	44.15 ± 0.41	53.17 ± 1.23
SP-N_2O (‰)	7.97 ± 1.48	7.56 ± 1.11	7.26 ± 0.92	9.31 ± 0.39	8.27 ± 1.36	14.10 ± 2.67	8.78 ± 1.59	6.66 ± 0.78	5.68 ± 0.49	11.26 ± 1.39	8.69 ± 1.78	15.43 ± 2.35

2.30 mg kg^{-1}), NO_2^- (58.71 ± 9.09 to 209.13 ± 32.04 μg kg^{-1}) and $\delta^{15}N\text{-}NO_3^-$ (16.10 ± 0.21 to 18.57 ± 0.69‰) in the study area (Table 1). The soil sulfide concentrations were in the range of 1.55 ± 0.70 to 105.73 ± 25.30 mg kg^{-1}, and the maximal concentration occurred at site D (Table 1). The $\delta^{15}N$ value of soil NH_4^+ (4.77 ± 1.58 to 9.52 ± 0.17‰) was significantly lower than that of NO_3^- and showed a decreasing trend from sites A to F. However, no significant spatial variation occurred for $\delta^{18}O\text{-}NO_3^-$ (−3.60 ± 0.99 to −1.51 ± 0.63‰) in the study area (Table 1). The soil potential NIT and DNF rates ranged from 0.08 ± 0.02 to 0.94 ± 0.04 nmol N g^{-1} h^{-1} and from 1.94 ± 0.20 to 29.87 ± 2.44 nmol N g^{-1} h^{-1}, respectively. Both the NIT and DNF potential rates were significantly higher in summer than in winter and increased from sites A to F (Fig. 3 and Table S3).

3.2. Soil N_2O emission rates and isotopic compositions

The soil N_2O emission rates varied from 0.70 ± 0.04 to 2.15 ± 0.12 μmol m^{-2} h^{-1} in the study area (Fig. 4), with relatively higher rates in summer and lower rates in winter ($p < 0.01$, Table S3). A remarkable spatial difference was observed in the N_2O emission rates, especially in summer (a site sequence of A < B ≈ C < E < F < D) ($p < 0.01$, Table S3 and Fig. 4).

The $\delta^{15}N$ and $\delta^{18}O$ values of emitted N_2O ranged from −4.49 ± 0.75 to 6.65 ± 0.33‰ and from 42.52 ± 0.34 to 53.17 ± 1.23‰, respectively (Fig. 4). Relatively higher $\delta^{15}N\text{-}N_2O$ values were observed at sites A (average of 4.63‰) and C (average of 1.06‰), while lower $\delta^{15}N\text{-}N_2O$ values were observed at sites B (average of −1.86‰), D (average of −2.42‰), E (average of −2.34‰) and F (average of −1.76‰). The values of $\delta^{18}O\text{-}N_2O$ were significantly higher in summer than in winter ($p < 0.05$). An increasing trend of $\delta^{18}O\text{-}N_2O$ was observed from sites A to F in summer, but the values were not significantly different in winter (Fig. 4). The SP-N_2O values varied from 7.26 ± 0.92 to 8.78 ± 1.59‰ in winter and from 6.66 ± 0.78 to 15.43 ± 2.35‰ in summer, and relatively higher SP values were observed at sites C and F (Fig. 4). The $\delta^{18}O\text{-}N_2O$ value was positively correlated with the SP-N_2O value and negatively correlated with $\delta^{15}N\text{-}N_2O$ ($p < 0.01$), while no significant correlation was observed between $\delta^{15}N\text{-}N_2O$ and SP-N_2O (Fig. S3).

3.3. Soil gross N_2O production and consumption rates

The gross N_2O production and consumption rates varied from 3.16 ± 0.09 to 14.34 ± 3.92 μmol m^{-2} h^{-1} and from 2.22 ± 0.08 to 12.54 ± 3.95 μmol m^{-2} h^{-1}, respectively, with significant spatial variability among the sampling sites (Fig. 5 and Table S3). In the summer, the gross N_2O production and consumption rates were generally higher at sites C, D, E and F than at sites A and B, but the rates did not significantly differ among the sites in the winter (Fig. 5). The N_2O consumption proportion ranged from 69.56 ± 2.25 to 90.31 ± 4.11% and exhibited a significant spatial difference ($p < 0.01$, Fig. 5 and Table S3). In the winter, the N_2O consumption proportion was generally lower at sites D, E and F than at sites A, B and C, although some differences were not significant (Fig. 5). Similarly, in the summer, a lower N_2O consumption proportion was also observed at sites D and E, except for site F (Fig. 5).

3.4. Soil N_2O production pathways

Natural-abundance isotope signature indicated that the majority of N_2O derived from bacterial DNF in the study area, which contributed approximately 78.22 to 97.36% of the gross N_2O production (Fig. 6). In contrast, NH_2OH oxidation contributed 2.64 to 21.78% of N_2O production (Fig. 6). A significant spatial variability among the sites was observed for the N_2O production pathways (Table S3). The contribution of NH_2OH oxidation to N_2O production generally showed an increasing trend from sites A to F, while the contribution of bacterial DNF showed a decreasing trend from sites A to F (Fig. 6).

4. Discussion

This study revealed new interesting details on the soil N_2O emission dynamics as well as their driving factors in estuarine and intertidal wetlands. The soil N_2O emission from estuarine and coastal wetlands is an important source of atmospheric N_2O (Usui et al., 2001; Dong et al., 2011). The magnitudes of N_2O emission (0.70 to 2.15 μmol m^{-2} h^{-1}) detected in the Yangtze estuarine and intertidal soils are comparable to those from other estuarine and coastal wetlands (Usui et al., 2001; Allen et al., 2011; Adams et al., 2012). In the present study, the N_2O emission rates varied significantly with the spatial location, and higher N_2O emissions were observed in the upper estuarine zones (sites D, E and F), especially in summer (Fig. 4). In general, the N_2O dynamics is mediated by both N_2O production and consumption processes, so it is difficult to discern the drivers only through the measurement of the N_2O emission rates (Yang and Silver, 2016). Here, we calculated the gross N_2O production and consumption rates based on emitted N_2O isotopic analysis (Toyoda et al., 2011; Ishii et al., 2014). It was actually found that the gross N_2O production and consumption rates in summer were higher at sites C, D, E and F than at sites A and B, while the rates did not significantly differ among the sites in winter (Fig. 5). N_2O consumption was quite pronounced, indicating that N_2O emission in such ecosystems accounts for only a small fraction of the total production (Vieten et al., 2007). Unlike gross N_2O production and consumption rates, lower consumption proportions generally occurred at the upper estuarine sites, although some differences were not significant (Fig. 5). Therefore, we can deduce that increased N_2O emission in the upper estuarine zones in the summer was primarily caused by higher gross N_2O production and lower N_2O consumption degree. Also, the small variations in

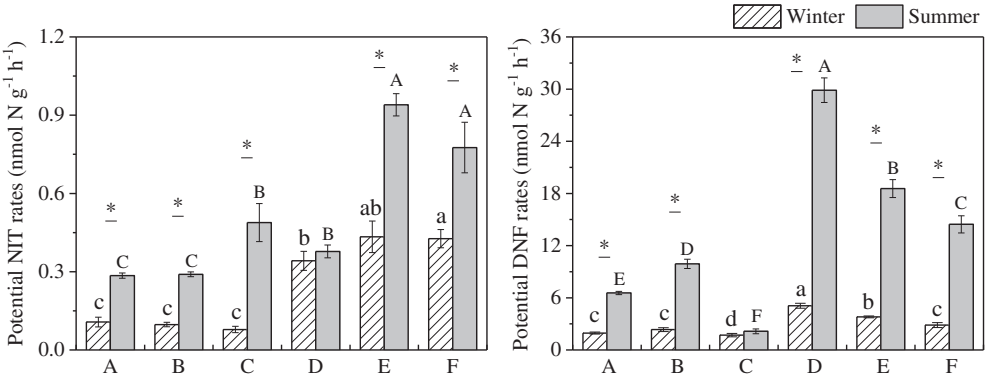

Fig. 3. Soil potential nitrification (NIT) and denitrification (DNF) rates. Error bars represent standard deviation ($n = 3$). Different lowercase and uppercase letters indicate significant spatial differences ($p < 0.05$), and the asterisks denote significant seasonal differences ($p < 0.05$).

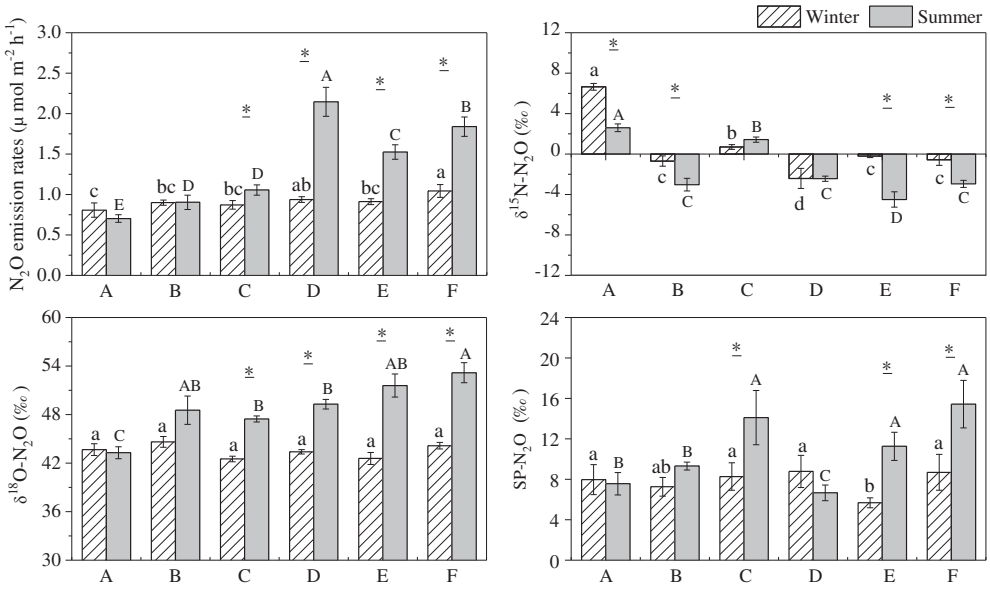

Fig. 4. N_2O emission rates and isotopic signatures. Error bars represent standard deviation ($n = 3$). Different lowercase and uppercase letters indicate significant spatial differences ($p < 0.05$), and the asterisks denote significant seasonal differences ($p < 0.05$).

gross N_2O production in the winter could explain why the spatial N_2O emission patterns were less pronounced compared with the summer. Notably, site C in the summer exhibited a higher gross N_2O production rate, and the unexpectedly lower N_2O emission at this site was mainly due to the larger N_2O consumption proportion (Fig. 5). These results indicated that gross N_2O production and consumption simultaneously drove the N_2O emission patterns across the estuarine and intertidal wetland (Park et al., 2011).

Gross N_2O production is mainly associated with soil NIT and/or DNF processes (Wrage et al., 2001; Bateman and Baggs, 2005). In this study, the potential rates of both NIT and DNF generally showed an increasing trend from sites A to F, especially in the summer (Fig. 3). Additionally, the availability of soil carbon and N substrates was also higher at sites D, E and F than at sites A, B and C (Table 1), likely because there were higher loadings of freshwater-derived terrestrial substrates at the upper estuarine sites (Maie et al., 2006). The increased concentrations of these substrates at sites D, E and F might enhance the NIT and/or DNF processes and thus contributed to the greater N_2O production (Usui et al., 2001; Park et al., 2011). Linear mixed models showed $N_2O_{emission}$ was significantly related to TOC and potential DNF rates, and $N_2O_{gross\ production}$ was also associated with DNF rates (Table S4). In addition, N_2O consumption plays a vital role in controlling N_2O emission, and it is favored in low-oxygen environments (Yang and Silver, 2016; Bourbonnais et al., 2017). Although we did not measure the oxygen availability, soil Fe^{2+}/Fe^{3+} ratios (2.14 ± 0.62 to 4.21 ± 1.19) implied that the study area was generally subjected to low-oxygen conditions (Battistuzzi et al., 2002; Li et al., 2003), which might lead to a relatively higher N_2O consumption. In the present study, N_2O consumption proportions were generally lower at the upper estuarine sites as noted above (Fig. 5). However, no similar spatial patterns of the Fe^{2+}/Fe^{3+} ratios were observed in this study, indicating that N_2O consumption was also influenced in part by other factors. For instance, the highest soil Fe^{2+}/Fe^{3+} ratios were observed at site D in both winter and summer (Table 1). This result might be because site D, located near the sewage outlet, experienced a highly concentrated wastewater input, which further affected the water quality and local redox conditions (Zhang et al., 2001). Based on the principles mentioned above, N_2O consumption degree at site D should be higher due to the strong reducing environment (Dalsgaard et al., 2014; Yang and Silver, 2016). Paradoxically, the lowest N_2O consumption proportion was observed here, which might be attributed to the inhibition of N_2O reduction by sulfide. It has been reported that high sulfide concentrations can directly inhibit N_2O reduction to N_2 (Sørensen et al., 1980; Brunet and Garcia-Gil, 1996). Indeed, the highest soil sulfide contents were observed at site D (Table 1), which likely explained the aforementioned phenomenon. Additionally, some studies have reported that low pH can suppress N_2O reductase activities and favor N_2O accumulation (Liu et al., 2010; Pan et al., 2012). In our study, the soil pH generally showed a decreasing trend from sites A to

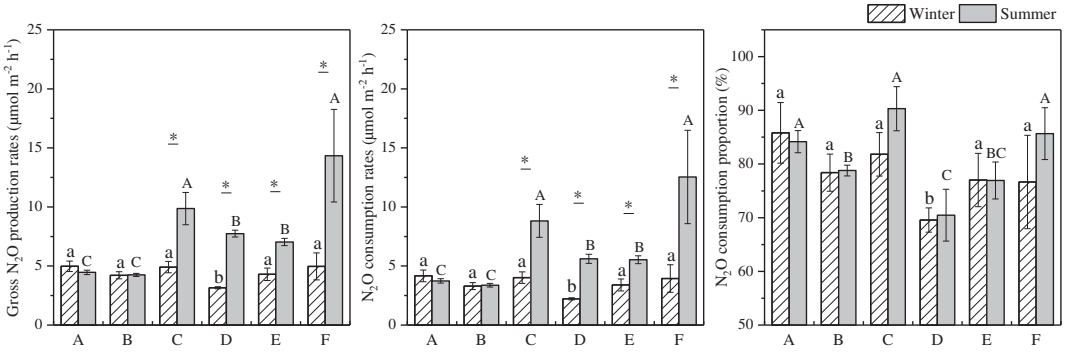

Fig. 5. Gross N_2O production and consumption rates as well as consumption proportion. Error bars represent standard deviation ($n = 3$). Different lowercase letters indicate significant spatial differences ($p < 0.05$), and the asterisks denote significant seasonal differences ($p < 0.05$).

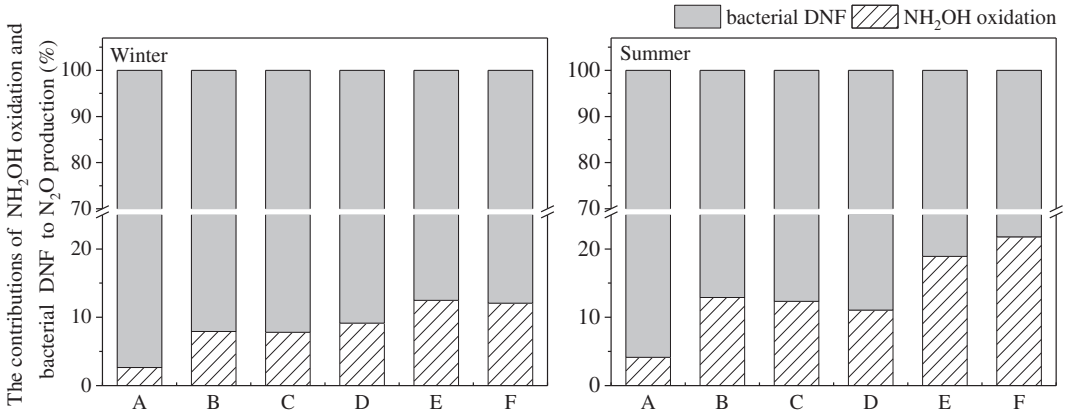

Fig. 6. Relative contributions of both NH_2OH oxidation and bacterial DNF to N_2O production.

F, which could also regulate the variations in N_2O consumption. However, no environmental variables were correlated with $N_2O_{consumtion}$, although $N_2O_{consumption\ proportion}$ was only related to mean particle size (Table S4). The lack of significant relationships likely implied that the underlying factors influencing N_2O consumption varied greatly among the Yangtze estuarine and intertidal wetlands (Yang and Silver, 2016). Seasonally, the N_2O emission rates were generally higher in the summer than in the winter (Fig. 4), likely because the high temperatures in the summer (approximately 32 °C) stimulated the NIT and DNF processes and led to higher N_2O production, compared with the winter (approximately 5 °C) (Schindlbacher et al., 2004; Allen et al., 2011). Overall, these environmental factors comprehensively affected the gross N_2O production and consumption in the estuarine and intertidal wetlands, and further regulated the variations of N_2O emissions.

The natural-abundance isotopes of the emitted N_2O ($\delta^{15}N$ and $\delta^{18}O$) can also shed light on the N_2O production processes (Toyoda et al., 2011; Zou et al., 2014). Our study indicated that the $\delta^{15}N$ values (-4.49 ± 0.75 to 6.65 ± 0.33‰) of the emitted N_2O in the Yangtze estuarine wetland were generally higher than those in cropland, grassland, forestland and peatland (Table S5), which can improve our understanding of the observed trends in the isotopic composition of the tropospheric N_2O (Toyoda et al., 2011). The $\delta^{15}N$-N_2O values varied considerably among the sites, and lower values were observed at sites B, D, E and F (Fig. 4). In general, the $\delta^{15}N$ value of the emitted N_2O was affected mainly by the substrate availability, precursor isotopic signatures and microbial processes of N_2O production and consumption (Pérez et al., 2001; Park et al., 2011). It has been reported that NIT process would lead to a greater depletion of ^{15}N in the produced N_2O, while N_2O reduction can enrich the isotopic signatures (Yoshida et al., 1984; Ostrom et al., 2000; Toyoda et al., 2011). Therefore, the decreased $\delta^{15}N$-N_2O values at sites B, D, E, and F might be attributed to a lower $\delta^{15}N$-NH_4^+ value and less N_2O reduction or a higher contribution of nitrification to N_2O production. Notably, the $\delta^{15}N$-NH_4^+ values were similar at sites B and C, but the $\delta^{15}N$-N_2O signatures were quite different at these two sites (Table 1 and Fig. 4). This result might be because larger N_2O reduction at site C caused the enrichment of ^{15}N in N_2O (Toyoda et al., 2011; Köster et al., 2013). Pérez et al. (2001) estimated the key N_2O production pathways by comparing the calculated enrichment factors $\varepsilon(^{15}N)$ (the difference between $\delta^{15}N$ values of the emitted N_2O and the substrate NH_4^+ or NO_3^-) with published values for different N_2O production processes. We also calculated $\varepsilon(^{15}N)$ for N_2O of each site, assuming that N_2O was produced either from NIT, DNF, nitrifier DNF or fungal DNF. Most of the calculated $\varepsilon(^{15}N)$ values were within the range of the published DNF enrichment factors, suggesting that DNF was the dominant pathway of N_2O production in the study area (Fig. S4). Nevertheless, the quantitative estimation of N_2O production based on the enrichment factors of $\delta^{15}N$ alone remains difficult because several uncertain processes occur simultaneously in natural ecosystems (Toyoda et al., 2011).

In addition, the variation of $\delta^{18}O$-N_2O is more complicated than $\delta^{15}N$-N_2O, because it is affected not only by the original O-atoms (NO_2^-, NO_3^-, soil water and O_2) and related N transformation processes, but also by O-isotope exchange with the soil water (Zou et al., 2014; Lewicka-Szczebak et al., 2016). In this study, the observed $\delta^{18}O$ values of N_2O varied from 42.39 to 53.17‰ and were higher than those of NO_3^- (-3.60 to 1.61‰). This result primarily resulted from O exchange with water and the enrichment of ^{18}O during N_2O reduction process (Lewicka-Szczebak et al., 2014; Zou et al., 2014). However, we only measured $\delta^{18}O$ of the substrate NO_3^-, and the information on the enrichment factors $\varepsilon(^{18}O)$ is limited. Therefore, the uncertainty remains for the identification of the O sources in the emitted N_2O (Park et al., 2011).

In contrast to $\delta^{15}N$ and $\delta^{18}O$ of N_2O, SP does not depend on the precursor isotope signatures, but on the microbial production and consumption processes of N_2O (Sutka et al., 2003). Numerous studies have confirmed that the SP value is a promising indicator for the identification of N_2O production pathways (Maeda et al., 2010; Zou et al., 2014; Gil et al., 2017). The SP values (6.66 ± 0.77 to 15.43 ± 2.53‰) of the emitted N_2O at our study sites are in the range of those obtained from other ecosystems (-39.8 to 58.0‰) (Table S5). In general, we would expect a positive correlation between $\delta^{15}N$-N_2O and $\delta^{18}O$-N_2O with SP-N_2O in the case of a pronounced N_2O reduction (Well et al., 2006). In this study, $\delta^{18}O$-N_2O was positively related to SP-N_2O ($r = 0.58$, $p < 0.05$), but no correlation was observed between $\delta^{15}N$-N_2O and SP-N_2O ($r = -0.22$, $p > 0.05$) (Fig. S3). These relationships indicated that the imprint from N_2O reduction might be masked by the N_2O production processes and its precursor isotope (Well et al., 2006). N_2O reduction often occurs in redox-dynamic environments, which affects the estimation of the N_2O production processes (Park et al., 2011; Ishii et al., 2014). To overcome this problem, the effect of N_2O reduction was considered based on SP and $\delta^{15}N$ of N_2O (Toyoda et al., 2011). In addition, the cycloheximide (CYH) addition experiments suggested that the N_2O production by fungi was low (Table S1). We thus assumed that the contribution of fungal DNF to N_2O production was negligible. Our results show that bacterial DNF was the dominant pathway (approximately 78 to 97%), and NH_2OH oxidation also contributed substantially to N_2O production (approximately 3 to 22%) (Fig. 6), which supports an earlier report suggesting N_2O production in intertidal soil was not only derived from DNF, but also from other N transformation processes (Wang et al., 2007). At present, it is difficult to distinguish the relative contributions of the nitrifier DNF and DNF processes to N_2O production based on SP values (Toyoda et al., 2011; Zou et al., 2014), so further studies should be conducted to solve this question and consider these processes separately to more robustly reveal their potential contributions to N_2O production.

The spatial variability of N_2O production processes was observed in intertidal wetlands of the Yangtze Estuary (Fig. 6), which could also be explained in part by soil environmental factors (Well et al., 2006; Köster et al., 2011; Park et al., 2011). Our results showed that $F_{NH_2OH\ oxidation}$ increased slightly across the Yangtze Estuary (from sites A to F), especially in the summer (Fig. 6). Theoretically, higher NH_4^+ concentrations can provide substrates for ammonia oxidation process and enhance N_2O production via NH_2OH oxidation pathway (Wunderlin et al., 2013; Ma et al., 2017). Indeed, higher NH_4^+ concentrations were observed at the upper estuarine sites (Table 1), which might lead to an increasing trend of $F_{NH_2OH\ oxidation}$ from sites A to F. Due to the kinetic isotope fraction effects, ammonia oxidation can result in an enrichment of ^{15}N in the residual NH_4^+ (Casciotti et al., 2003; Well et al., 2006). Base on this principle, higher $\delta^{15}N$-NH_4^+ signatures should also be observed at the upper estuarine sites, but it was not the case (Table 1). One possible explanation for this result was that soil NH_4^+ in upper estuarine zones derived greatly from organic matter mineralization (Wu et al., 2015; Murray et al., 2018). In addition, the highest $F_{NH_2OH\ oxidation}$ was not observed at site D, although the maximal NH_4^+ concentration was detected there, which might be attributed to the limitation of the oxygen level (Ma et al., 2017). The mechanism of the pH influence on ammonia oxidation contribution to N_2O production is not well understood, but previous studies show that the potential NIT rates are negatively related to the pH (Hu et al., 2015). Thus, an increasing tendency of $F_{NH_2OH\ oxidation}$ along the decreasing soil pH gradient (from sites A to F) can be postulated. In this study, only soil bulk density was found to be associated with $F_{NH_2OH\ oxidation}$ (Table S4), which also indicated that the factors influencing $F_{NH_2OH\ oxidation}$ were various. In contrast, $F_{bacterial\ DNF}$ generally showed a decreasing trend from sites A to F (Fig. 6). However, we did not distinguish the relative importance of nitrifier DNF and DNF to N_2O production, and the underlying mechanisms affecting the variations in bacterial DNF should be further explored.

Notably, the results of our experiment represent a snapshot of soil N_2O emission dynamics in the estuarine and intertidal wetlands. However, the environmental conditions in these ecosystems vary greatly due to the tidal action, which could affect the N dynamic on a time scale of several hours (Capooci et al., 2019). Meanwhile, a relatively long-term incubation (such as 6 h) in this study might change the pressure within the static chambers, which could also influence the N_2O emission (Lund et al., 1999). Considering these limitations, our future efforts should be improved by in situ field experiments and increasing temporal coverage, which may help discern the high variability of N_2O emission under the tidal cycle. In addition, N_2O source partitioning based on isotopic signatures is probably approximate, and the future study is required to combine with other complementary approaches (Ishii et al., 2014; Duan et al., 2017). Nevertheless, natural-abundance isotopes provide valuable information about the N_2O dynamics in estuarine and coastal wetlands, which helps us understand the drivers of N_2O emission.

5. Conclusion

This study revealed the N_2O emission dynamics in the soils of estuarine and intertidal wetlands. The N_2O emission rates were driven by the gross N_2O production and consumption processes simultaneously, with a significant spatio-temporal variation. N_2O consumption was quite pronounced in such ecosystems, indicating that N_2O emission accounts for only a small fraction of the total production. NH_2OH oxidation (2.42–26.23%) was of substantial importance in N_2O production, even though bacteria DNF (78.22–97.36%) was the dominant microbial pathway. Soil pH, Fe^{2+}/Fe^{3+}, and sulfide and substrate availability were the underlying factors influencing the N_2O production and consumption processes. Overall, this study provides a valuable perspective on the mechanisms controlling N_2O cycling and illustrates that the natural isotope analyses are promising tools for identifying the N_2O dynamics in estuarine and intertidal ecosystems.

Declaration of competing interest

The authors declare that they have no known competing financial interests or personal relationships that could have appeared to influence the work reported in this paper.

Acknowledgments

This work was funded by the Natural Science Foundation of China (grant numbers: 41725002, 41671463, 41761144062, and 41730646). It was also supported by Chinese National Key Programs for Fundamental Research and Development (No. 2016YFA0600904 and 2016YFE0133700), Fundamental Research Funds for the Central Universities, and the Yangtze Delta Estuarine Wetland Station (ECNU). Many thanks are given to Wayne S. Gardner, Kaijun Lu, anonymous reviewers and editor for constructive comments and valuable suggestions on this manuscript.

Appendix A. Supplementary data

Supplementary data to this article can be found online at https://doi.org/10.1016/j.scitotenv.2020.137073.

References

Adams, C.A., Andrews, J.E., Jickells, T., 2012. Nitrous oxide and methane fluxes vs. carbon, nitrogen and phosphorous burial in new intertidal and saltmarsh sediments. Sci. Total Environ. 434, 240–251.

Allen, D., Dalal, R.C., Rennenberg, H., Schmidt, S., 2011. Seasonal variation in nitrous oxide and methane emissions from subtropical estuary and coastal mangrove sediments, Australia. Plant Biol. 13, 126–133.

Amouroux, D., Roberts, G., Rapsomanikis, S., Andreae, M.O., 2002. Biogenic gas (CH_4, N_2O, DMS) emission to the atmosphere from near-shore and shelf waters of the northwestern Black Sea. Estuar. Coast. Shelf Sci. 54, 575–587.

Bateman, E.J., Baggs, E.M., 2005. Contributions of nitrification and denitrification to N_2O emissions from soils at different water-filled pore space. Biol. Fertil. Soils 41, 379–388.

Battistuzzi, G., Borsari, M., Ranieri, A., Sola, M., 2002. Redox thermodynamics of the Fe^{3+}/Fe^{2+} couple in horseradish peroxidase and its cyanide complex. J. Am. Chem. Soc. 124, 26–27.

Bourbonnais, A., Letscher, R.T., Bange, H.W., Echevin, V., Larkum, J., Mohn, J., Yoshida, N., Altabet, M.A., 2017. N_2O production and consumption from stable isotopic and concentration data in the Peruvian coastal upwelling system. Glob. Biogeochem. Cycles 31, 678–698.

Breider, F., Yoshikawa, C., Abe, H., Toyoda, S., Yoshida, N., 2015. Origin and fluxes of nitrous oxide along a latitudinal transect in western North Pacific: controls and regional significance. Glob. Biogeochem. Cycles 29, 1014–1027.

Brunet, R.C., Garcia-Gil, L.J., 1996. Sulfide-induced dissimilatory nitrate reduction to ammonia in anaerobic freshwater sediments. FEMS Microbiol. Ecol. 21 (2), 131–138.

Butterbach-Bahl, K., Baggs, E.M., Dannenmann, M., Kiese, R., Zechmeister-Boltenstern, S., 2013. Nitrous oxide emissions from soils: how well do we understand the processes and their controls? Philos. Trans. R. Soc. B 368, 20130122.

Capooci, M., Barba, J., Seyfferth, A.L., Vargas, R., 2019. Experimental influence of storm-surge salinity on soil greenhouse gas emissions from a tidal salt marsh. Sci. Total Environ. 686, 1164–1172.

Casciotti, K.L., Sigman, D.M., Ward, B.B., 2003. Linking diversity and stable isotope fractionation in ammonia-oxidizing bacteria. Geomicrobiol J. 20 (4), 335–353.

Cline, J.D., 1969. Spectrophotometric determination of hydrogen sulfide in natural waters. Limnol. Oceanogr. 14, 454–458.

Dalsgaard, T., Stewart, F.J., Thamdrup, B., De Brabandere, L., Revsbech, N.P., Ulloa, O., Canfield, D.E., DeLong, E.F., 2014. Oxygen at nanomolar levels reversibly suppresses process rates and gene expression in anammox and denitrification in the oxygen minimum zone off northern Chile. MBio 5 (6) (e01966-14).

Deng, F.Y., Hou, L.J., Liu, M., Zheng, Y.L., Yin, G.Y., Li, X.F., Lin, X.B., Chen, F., Gao, J., Jiang, X.F., 2015. Dissimilatory nitrate reduction processes and associated contribution to nitrogen removal in sediments of the Yangtze estuary. J. Geophys. Res. Biogeosci. 120, 1521–1531.

Deppe, M., Well, R., Giesemann, A., Spott, O., Flessa, H., 2017. Soil N_2O fluxes and related processes in laboratory incubations simulating ammonium fertilizer depots. Soil Biol. Biochem. 104, 68–80.

Dong, L.F., Sobey, M.N., Smith, C.J., Rusmana, I., Phillips, W., Stott, A., Mark Osborn, A., Nedwell, D., 2011. Dissimilatory reduction of nitrate to ammonium, not denitrification or anammox, dominates benthic nitrate reduction in tropical estuaries. Limnol. Oceanogr. 56, 279–291.

Duan, H., Ye, L., Erler, D., Ni, B.J., Yuan, Z.G., 2017. Quantifying nitrous oxide production pathways in wastewater treatment systems using isotope technology–a critical review. Water Res. 122, 96–113.

Gao, D.Z., Li, X.F., Lin, X.B., Wu, D.M., Jin, B.S., Huang, Y.P., Liu, M., Chen, X., 2017. Soil dissimilatory nitrate reduction processes in the *Spartina alterniflora* invasion

chronosequences of a coastal wetland of southeastern China: dynamics and environmental implications. Plant Soil 421, 383–399.
Gil, J., Pérez, T., Boering, K., Martikainen, P.J., Biasi, C., 2017. Mechanisms responsible for high N_2O emissions from subarctic permafrost peatlands studied via stable isotope techniques. Glob. Biogeochem. Cycles 31, 172–189.
Gong, Y., Wu, J., Vogt, J., Le, T.B., 2019. Warming reduces the increase in N_2O emission under nitrogen fertilization in a boreal peatland. Sci. Total Environ. 664, 72–78.
Granger, J., Sigman, D.M., 2009. Removal of nitrite with sulfamic acid for nitrate N and O isotope analysis with the denitrifier method. Rapid Commun. Mass Spectrom. 23, 3753–3762.
Hou, L., Zheng, Y., Liu, M., Gong, J., Zhang, X., Yin, G., You, L., 2013. Anaerobic ammonium oxidation (anammox) bacterial diversity, abundance, and activity in marsh sediments of the Yangtze Estuary. J. Geophys. Res. Biogeosci. 118, 1237–1246.
Hu, H.W., Chen, D., He, J.Z., 2015. Microbial regulation of terrestrial nitrous oxide formation: understanding the biological pathways for prediction of emission rates. FEMS Microbiol. Rev. 39, 729–749.
IPCC, 2013. Climate Change 2013: The Physical Science Basis. Cambridge University Press, Cambridge.
Ishii, S., Song, Y., Rathnayake, L., Tumendelger, A., Satoh, H., Toyoda, S., Okabe, S., 2014. Identification of key nitrous oxide production pathways in aerobic partial nitrifying granules. Environ. Microbiol. 16, 3168–3180.
Köster, J.R., Cárdenas, L., Senbayram, M., Bol, R., Well, R., Butler, M., Dittert, K., 2011. Rapid shift from denitrification to nitrification in soil after biogas residue application as indicated by nitrous oxide isotopomers. Soil Biol. Biochem. 43, 1671–1677.
Köster, J.R., Well, R., Dittert, K., Giesemann, A., Lewicka-Szczebak, D., Mühling, K.H., Herrmann, A., Lammel, J., Senbayram, M., 2013. Soil denitrification potential and its influence on N_2O reduction and N_2O isotopomer ratios. Rapid Commun. Mass Spectrom. 27 (21), 2363–2373.
Kozlowski, J.A., Price, J., Stein, L.Y., 2014. Revision of N_2O-producing pathways in the ammonia-oxidizing bacterium *Nitrosomonas europaea* ATCC 19718. Appl. Environ. Microbiol. 80, 4930–4935. https://doi.org/10.1128/AEM.01061-14.
Kurola, J., Salkinoja-Salonen, M., Aarnio, T., Hultman, J., Romantschuk, M., 2005. Activity, diversity and population size of ammonia-oxidising bacteria in oil-contaminated landfarming soil. FEMS Microbiol. Lett. 250, 33–38.
Lewicka-Szczebak, D., Well, R., Köster, J.R., Fuß, R., Senbayram, M., Dittert, K., Flessa, H., 2014. Experimental determinations of isotopic fractionation factors associated with N2O production and reduction during denitrification in soils. Geochim. Cosmochim. Acta 134, 55–73.
Lewicka-Szczebak, D., Dyckmans, J., Kaiser, J., Marca, A., Augustin, J., Well, R., 2016. Oxygen isotope fractionation during N_2O production by soil denitrification. Biogeosciences 13, 1129.
Li, X.G., Lv, X.X., Sun, Y.M., Li, N., Yuan, M.H., Zhan, T.L., Song, J.M., 2003. Relation of active iron and redox environments in the sediments of Bohai Sea. Mar. Environ. Sci. 22, 20–24.
Liu, C.Y., Zheng, X.H., Zhou, Z.X., Han, S.H., Wang, Y.H., Wang, K., Liang, W.G., Li, M., Chen, D.L., Yang, Z.P., 2010. Nitrous oxide and nitric oxide emissions from an irrigated cotton field in Northern China. Plant Soil 332, 123–134.
Lund, C.P., Riley, W.J., Pierce, L.L., Field, C.B., 1999. The effects of chamber pressurization on soil-surface CO_2 flux and the implications for NEE measurements under elevated CO_2. Glob. Chang. Biol. 5 (3), 269–281.
Ma, C., Jensen, M.M., Smets, B.F., Thamdrup, B., 2017. Pathways and controls of N_2O production in nitritation–anammox biomass. Environ. Sci. Technol. 51, 8981–8991.
Maeda, K., Toyoda, S., Shimojima, R., Osada, T., Hanajima, D., Morioka, R., Yoshida, N., 2010. Source of nitrous oxide emissions during the cow manure composting process as revealed by isotopomer analysis of and *amoA* abundance in betaproteobacterial ammonia-oxidizing bacteria. Appl. Environ. Microbiol. 76, 1555–1562.
Maeda, K., Toyoda, S., Philippot, L., Hattori, S., Nakajima, K., Ito, Y., Yoshida, N., 2017. Relative contribution of *nirK*- and *nirS*- bacterial denitrifiers as well as fungal denitrifiers to nitrous oxide production from dairy manure compost. Environ. Sci. Technol. 51, 14083–14091.
Maie, N., Boyer, J.N., Yang, C., Jaffe, R., 2006. Spatial, geomorphological, and seasonal variability of CDOM in estuaries of the Florida Coastal Everglades. Hydrobiologia 569, 135–150.
McIlvin, M.R., Casciotti, K.L., 2011. Technical updates to the bacterial method for nitrate isotopic analyses. Anal. Chem. 83, 1850–1856.
Moseman-Valtierra, S., Gonzalez, R., Kroeger, K.D., Tang, J., Chao, W.C., Crusius, J., Bratton, J., Green, A., Shelton, J., 2011. Short-term nitrogen additions can shift a coastal wetland from a sink to a source of N_2O. Atmos. Environ. 45, 4390–4397.
Murray, R., Erler, D., Rosentreter, J., Maher, D., Eyre, B., 2018. A seasonal source and sink of nitrous oxide in mangroves: Insights from concentration, isotope, and isotopomer measurements. Geochim. Cosmochim. Acta 238, 169–192.
Musenze, R.S., Werner, U., Grinham, A., Udy, J., Yuan, Z., 2014. Methane and nitrous oxide emissions from a subtropical estuary (the Brisbane River estuary, Australia). Sci. Total Environ. 472, 719–729.
Osland, M.J., Enwright, N., Day, R.H., Doyle, T.W., 2013. Winter climate change and coastal wetland foundation species: salt marshes vs. mangrove forests in the southeastern United States. Glob. Chang. Biol. 19, 1482–1494.
Ostrom, N.E., Russ, M.E., Popp, B., Rust, T.M., Karl, D.M., 2000. Mechanisms of nitrous oxide production in the subtropical North Pacific based on determinations of the isotopic abundances of nitrous oxide and di-oxygen. Chemosphere Global Change Sci. 2, 281–290.
Ostrom, N.E., Pitt, A., Sutka, R., Ostrom, P.H., Grandy, A.S., Huizinga, K.M., Robertson, G.P., 2007. Isotopologue effects during N_2O reduction in soils and in pure cultures of denitrifiers. J. Geophys. Res. Biogeosci. 112.
Pan, Y., Ye, L., Ni, B.J., Yuan, Z., 2012. Effect of pH on N_2O reduction and accumulation during denitrification by methanol utilizing denitrifiers. Water Res. 46, 4832–4840.
Park, S., Perez, T., A Boering, K., Trumbore, S.E., Gil, J., Marquina, S., Tyler, S.C., 2011. Can N_2O stable isotopes and isotopomers be useful tools to characterize sources and microbial pathways of N_2O production and consumption in tropical soils? Glob. Biogeochem. Cycles 25, 1–16.
Pérez, T., Trumbore, S.E., Tyler, S.C., Matson, P.A., Ortiz-Monasterio, I., Rahn, T., Griffith, D.W.T., 2001. Identifying the agricultural imprint on the global N_2O budget using stable isotopes. J. Geophys. Res. Atmos. 106, 9869–9878.
Prather, M.J., Hsu, J., DeLuca, N.M., Jackman, C.H., Oman, L.D., Douglass, A.R., Fleming, E.L., Strahan, S.E., Steenrod, S.D., Søvde, O.A., Isaksen, I.S.A., Froidevaux, L., Funke, B., 2015. Measuring and modeling the lifetime of nitrous oxide including its variability. J. Geophys. Res.-Atmos. 120 (11), 5693–5705.
Quick, A.M., Reeder, W.J., Farrell, T.B., Tonina, D., Feris, K.P., Benner, S.G., 2019. Nitrous oxide from streams and rivers: a review of primary biogeochemical pathways and environmental variables. Earth Sci. Rev. 191, 224–262.
R Core Team, 2015. R: A Language and Environment for Statistical Computing. http://www.R-project.org/.
Ravishankara, A.R., Daniel, J.S., Portmann, R.W., 2009. Nitrous oxide (N_2O): the dominant ozone-depleting substance emitted in the 21st century. Science 326, 123–125.
Schindlbacher, A., Zechmeister-Boltenstern, S., Butterbach-Bahl, K., 2004. Effects of soil moisture and temperature on NO, NO_2, and N_2O emissions from European forest soils. J. Geophys. Res. Atmos. 109.
Song, Y.Y., Song, C.C., Yang, G.S., Miao, Y.Q., Wang, J.Y., Guo, Y.D., 2012. Changes in labile organic carbon fractions and soil enzyme activities after marshland reclamation and restoration in the Sanjiang Plain in Northeast China. Environ. Manag. 50, 418–426.
Sørensen, J., Tiedje, J.M., Firestone, R.B., 1980. Inhibition by sulfide of nitric and nitrous oxide reduction by denitrifying *Pseudomonas fluorescens*. Appl. Environ. Microbiol. 39, 105–108.
Sun, Z.G., Wang, L.L., Tian, H., Jiang, H.Q., Mou, X.J., Sun, W.G., 2013. Fluxes of nitrous oxide and methane in different coastal *Suaeda salsa* marshes of the Yellow River estuary, China. Chemosphere 90, 856–865.
Sutka, R.L., Ostrom, N.E., Ostrom, P.H., Gandhi, H., Breznak, J.A., 2003. Nitrogen isotopomer site preference of N_2O produced by *Nitrosomonas europaea* and *Methylococcus capsulatus* Bath. Rapid Commun. Mass Spectrom. 17, 738–745.
Sutka, R.L., Ostrom, N.E., Ostrom, P.H., Gandhi, H., Breznak, J.A., 2004. Nitrogen isotopomer site preference of N_2O produced by *Nitrosomonas europaea* and *Methylococcus capsulatus* Bath. Rapid Commun. Mass Spectrom. 18, 1411–1412.
Sutka, R.L., Ostrom, N.E., Ostrom, P.H., Breznak, J.A., Gandhi, H., Pitt, A.J., Li, F., 2006. Distinguishing nitrous oxide production from nitrification and denitrification on the basis of isotopomer abundances. Appl. Environ. Microbiol. 72, 638–644. https://doi.org/10.1128/AEM.72.1.638-644.2006.
Sutka, R.L., Adams, G.C., Ostrom, N.E., Ostrom, P.H., 2008. Isotopologue fractionation during N_2O production by fungal denitrification. Rapid Commun. Mass Spectrom. 22, 3989–3996.
Thamdrup, B., Dalsgaard, T., 2002. Production of N_2 through anaerobic ammonium oxidation coupled to nitrate reduction in marine sediments. Appl. Environ. Microbiol. 68, 1312–1318.
Tong, C., Huang, J.F., Hu, Z.Q., Jin, Y.F., 2013. Diurnal variations of carbon dioxide, methane, and nitrous oxide vertical fluxes in a subtropical estuarine marsh on neap and spring tide days. Estuar. Coasts 36, 633–642.
Toyoda, S., Yoshida, N., 1999. Determination of nitrogen isotopomers of nitrous oxide on a modified isotope ratio mass spectrometer. Anal. Chem. 71, 4711–4718.
Toyoda, S., Mutobe, H., Yamagishi, H., Yoshida, N., Tanji, Y., 2005. Fractionation of N_2O isotopomers during production by denitrifier. Soil Biol. Biochem. 37, 1535–1545.
Toyoda, S., Yano, M., Nishimura, S.I., Akiyama, H., Hayakawa, A., Koba, K., Sudo, S., Yagi, K., Makabe, A., Tobari, Y., Ogawa, N.O., Ohkouchi, N., Yamada, K., Yoshida, N., 2011. Characterization and production and consumption processes of N_2O emitted from temperate agricultural soils determined via isotopomer ratio analysis. Glob. Biogeochem. Cycles 25. https://doi.org/10.1029/2009GB003769.
Usui, T., Koike, I., Ogura, N., 2001. N_2O production, nitrification and denitrification in an estuarine sediment. Estuar. Coast. Shelf Sci. 52, 769–781.
Verhoeven, E., Barthel, M., Yu, L., Celi, L., Said-Pullicino, D., Sleutel, S., Lewicka-Szczebak, D., Six, J., Decock, C., 2019. Early season N_2O emissions under variable water management in rice systems: source-partitioning emissions using isotope ratios along a depth profile. Biogeosciences 16 (2), 383–408.
Vieten, B., Conen, F., Seth, B., Alewell, C., 2007. The fate of N_2O consumed in soils. Biogeosciences 4 (5), 3331–3341.
Wang, D.Q., Chen, Z.L., Wang, J., Xu, S.Y., Yang, H.X., Chen, H., Yang, L.Y., Hu, L.Z., 2007. Summer-time denitrification and nitrous oxide exchange in the intertidal zone of the Yangtze Estuar. Coast. Shelf Sci. 73, 43–53.
Well, R., Kurganova, I., de Gerenyu, V.L., Flessa, H., 2006. Isotopomer signatures of soil-emitted N_2O under different moisture conditions—a microcosm study with arable loess soil. Soil Biol. Biochem. 38, 2923–2933.
Wenk, C.B., Frame, C.H., Koba, K., Casciotti, K.L., Veronesi, M., Niemann, H., Zopfi, J., 2016. Differential N_2O dynamics in two oxygen-deficient lake basins revealed by stable isotope and isotopomer distributions. Limnol. Oceanogr. 61, 1735–1749. https://doi.org/10.1002/lno.10329.
Westley, M.B., Yamagishi, H., Popp, B.N., Yoshida, N., 2006. Nitrous oxide cycling in the Black Sea inferred from stable isotope and isotopomer distributions. Deep Sea Res., Part II 53, 1802–1816.
Wolf, B., Merbold, L., Decock, C., Tuzson, B., Harris, E., Six, J., Mohn, J., 2015. First on-line isotopic characterization of N_2O above intensively managed grassland. Biogeosciences 12, 2517–2531. https://doi.org/10.5194/bg-12-2517-2015.
Wrage, N., Velthof, G.L., Van Beusichem, M.L., Oenema, O., 2001. Role of nitrifier denitrification in the production of nitrous oxide. Soil Biol. Biochem. 33, 1723–1732.

Wu, Q.L., Ruan, X.H., Wu, C.M., Li, R.F., Wang, C.W., Wan, Y., 2015. Analyses of sources and transformation of nitrogen as a contaminant in the river and lake water in the western region of the Taihu Lake basin. Acta Sci. Circumst. 35 (12), 3883–3889.

Wunderlin, P., Lehmann, M.F., Siegrist, H., Tuzson, B., Joss, A., Emmenegger, L., Mohn, J., 2013. Isotope signatures of N_2O in a mixed microbial population system: constraints on N_2O producing pathways in wastewater treatment. Environ. Sci. Technol. 47, 1339–1348.

Yang, W.H., Silver, W.L., 2016. Gross nitrous oxide production drives net nitrous oxide fluxes across a salt marsh landscape. Glob. Chang. Biol. 22, 2228–2237.

Yin, G.Y., Hou, L.J., Liu, M., Li, X.F., Zheng, Y.L., Gao, J., Lin, X.B., 2017. DNRA in intertidal sediments of the Yangtze Estuary. J. Geophys. Res. Biogeosci. 122, 1988–1998.

Yoshida, N., 1988. ^{15}N-depleted N_2O as a product of nitrification. Nature 335, 528.

Zhang, W., Yu, L., Hutchinson, S.M., Xu, S., Chen, Z., Gao, X., 2001. China's Yangtze Estuary: I. Geomorphic influence on heavy metal accumulation in intertidal sediments. Geomorphology 41, 195–205.

Zhang, W.L., Zeng, C.S., Tong, C., Zhai, S.J., Lin, X., Gao, D.Z., 2015. Spatial distribution of phosphorus speciation in marsh sediments along a hydrologic gradient in a subtropical estuarine wetland, China. Estuar. Coast. Shelf Sci. 154, 30–38.

Yoshida, N., Hattori, A., Saino, T., Matsuo, S., Wada, E., 1984. $^{15}N/^{14}N$ ratio of dissolved N_2O in the eastern tropical Pacific Ocean. Nature 307, 442–444.

Zhang, W., Li, Y.Z., Xu, C.Y., Li, Q.Z., Lin, W., 2016. Isotope signatures of N_2O emitted from vegetable soil: ammonia oxidation drives N_2O production in NH_4^+-fertilized soil of North China. Sci. Rep. 6, 29257.

Zheng, Y.L., Hou, L.J., Liu, M., Gao, J., Yin, G.Y., Li, X.F., Lin, X.B., Jiang, X.F., Chen, F., Zong, H.B., Zhou, J.L., 2015. Diversity, abundance, and distribution of *nirS*-harboring denitrifiers in intertidal sediments of the Yangtze Estuary. Microb. Ecol. 70, 30–40.

Zhu, X., Burger, M., Doane, T.A., Horwath, W.R., 2013. Ammonia oxidation pathways and nitrifier denitrification are significant sources of N_2O and NO under low oxygen availability. Proc. Natl. Acad. Sci. U. S. A. 110, 6328–6333.

Zou, Y., Hirono, Y., Yanai, Y., Hattori, S., Toyoda, S., Yoshida, N., 2014. Isotopomer analysis of nitrous oxide accumulated in soil cultivated with tea (*Camellia sinensis*) in Shizuoka, central Japan. Soil Biol. Biochem. 77, 276–291.

Zuur, A.F., Ieno, E.N., Elphick, C.S., 2010. A protocol for data exploration to avoid common statistical problems. Methods Ecol. Evol. 1 (1), 3–14.